Structure, Raman scattering, and transport properties of boron-doped graphite

Y. Hishiyama, H. Irumano, and Y. Kaburagi
Faculty of Engineering, Musashi Institute of Technology, Setagaya-ku, Tokyo 158-8557, Japan

Y. Soneda
National Institute for Resources and Environment, Tsukuba, Ibaraki 305-8569, Japan

(Received 29 September 2000; revised manuscript received 31 January 2001; published 31 May 2001)

Boron-doped highly oriented graphite films (B-HOGF's) with an atomic fraction of boron from 0.4 up to 2.2 at. % have been prepared from well-crystallized, highly oriented graphite. The effect of boron doping on crystal structure has been investigated in terms of texture observation with a field-emission gun-type scanning electron microscope and by measurements of the x-ray diffraction and Raman scattering. The results indicate that in B-HOGF's, boron atoms substituted in the graphite lattice and induced disorder, which caused the Raman bands related to the disorder in graphite layer planes to appear. For each of the B-HOGF's, the temperature dependence of the resistivity in a range 1.8–300 K has been measured. The Hall coefficient and transverse magnetoresistance have also been measured at 3.0 K in a magnetic field range up to 4 T. The Hall coefficient data indicate that each of the B-HOGF's is a mixed crystal of graphite grains with and without boron atoms. The temperature dependence of the resistivity and field dependence of the transverse magnetoresistance for B-HOGF's show a characteristic that is possibly explained by a three-dimensional weak localization theory proposed by Sugihara Hishiyama, and Kaburagi.

DOI: 10.1103/PhysRevB.63.245406 PACS number(s): 68.55.Jk, 61.10.−i, 81.15.−z, 78.30.−j

I. INTRODUCTION

The present paper concerns the structure and transport properties of boron-doped graphite related to disorder induced by boron doping. Boron atoms can dissolve into the graphite lattice with a maximum solid solubility of 2.35 at. % boron at 2350 °C.[1] Within the solubility limit, the lattice constant a_0 increases linearly with increasing boron content x_B, while c_0 decreases linearly, though both variations are slight.[1] Hagio, Nakamizo, and Kobayashi studied the structural evolution of purified China natural graphite mixed with 0.6 wt. % boron by heat treatment at various temperatures between 1400 and 2700 °C for 1 h.[2] In their x-ray diffraction study on the samples heat-treated above 2400 °C, they concluded that these boron-doped graphite samples were composed of large crystallites with a fairly high crystal perfection, but the lattice constants are slightly different from those of undoped pristine graphite with slight elongation of a_0, but with slightly contradicting c_0. They also measured Raman spectra of the boron-doped graphite specimens using 514.5-nm excitation. All of the boron-doped graphites showed the intense 1360-cm^{-1} band (D mode) and the weak but sharp 1618-cm^{-1} band (D' mode) at the higher-frequency side of the strong 1589-cm^{-1} band (G mode); these bands are known to be caused by lattice disorder.[3–6] It was concluded that boron doping introduced a significant amount of structural defects into the graphite lattice, which contradicted the x-ray result.

A boron atom has three valence electrons, and the boron atom substituted into the graphite lattice traps an electron from the conduction band and lowers the Fermi level. Soule studied the effect of the depression of the Fermi level by boron doping on the transport properties,[7] being based on the energy band model of graphite. He observed a negative transverse magnetoresistance at liquid-nitrogen temperature for specimens with atomic fractions of boron with $x_B \geqslant 0.5$ at. %, but he did not give a detailed explanation. Hishiyama, Mrozowski, and Vagh also found a negative transverse magnetoresistance at liquid-nitrogen temperature for specimens of boron-doped Kish graphite, but they did not carry out any structural study.[8] The negative transverse magnetoresistance observed for the boron-doped graphite materials seems to be due to the disorder induced in the graphite lattice by boron doping.

Commercially available graphite materials have graphite structure but they are rather defective if we compare their crystal structure with those of highly crystallized graphite materials such as a single crystal, Kish graphite, and highly oriented pyrolytic graphite (HOPG). A commercially available graphite film named Grafoil is an example of a well-crystallized graphite film having almost the same crystallinity as natural graphite but with lower crystallinity than those of highly crystallized graphite materials. Koike *et al.* carried out detailed measurements on the resistivity ρ and magnetoresistance $\Delta\rho/\rho_0$ for specimens of Grafoil at very low temperatures below 1 K and in magnetic fields up to 0.4 T.[9] They found anomalous behavior for the specimens represented by

$$\rho(T) = \rho(0) - a\sqrt{T} \tag{1}$$

and

$$\Delta\rho/\rho_0 = -b\sqrt{B}, \tag{2}$$

where $\rho(T)$ and $\rho(0)$ are the resistivity at temperature T and that at 0 K, a is a positive constant, B is the magnetic field, and b is a positive constant. These results were explained fairly well in terms of localization, the electron-electron interaction, and the ellipsoidal band in the three-dimensional (3D) weak localization. The $\sqrt{T}$ dependence of the resistivity

TABLE I. Boron-doping treatments for graphite films, the lattice constants a_0 and c_0, the atomic fraction of boron dissolved into the graphite lattice x_B, the full width at half maximum of the peak intensity recording of the 002 diffraction $\phi_{1/2}$, room-temperature resistivity $\rho_{300\,K}$, resistivity ratio $\rho_{300\,K}/\rho_{3\,K}$, and transverse magnetoresistance measured at 3 K in a field of 1 T, $(\Delta\rho/\rho_0)_{3\,K,1\,T}$ for HOGF and B-HOGF's.

Sample	Doping treatment	Second heat treatment	a_0 (nm)	c_0 (nm)	x_B (at. %)	$\varphi_{1/2}$ (deg)	$\rho_{300\,K}$ ($10^7\ \Omega$ m)	$\rho_{300\,K}/\rho_{3\,K}$	$(\Delta\rho/\rho_0)_{3\,K,1\,T}$ (%)
HOGF			0.246 12	0.670 76	0	4.04	6.33	1.13	901
B-HOGF-0.4	2350 °C for 5 min	2600 °C for 10 sec	0.246 23	0.670 54	0.4	4.62	13.0	1.0391	0.137
B-HOGF-0.5	2350 °C for 5 min	2550 °C for 10 sec		0.670 46	0.5		14.2	0.9911	0.003
B-HOGF-0.9	2350 °C for 5 min	2500 °C for 10 sec		0.670 22	0.9		19.5	0.9735	−0.183
B-HOGF-1.4	2350 °C for 5 min	2450 °C for 10 sec		0.669 92	1.4		24.8	0.9645	−0.179
B-HOGF-2.2	2500 °C for 2 h		0.246 82	0.669 44	2.2	10.23	26.4	0.9785	−0.169

and negative $\sqrt{B}$ magnetoresistance at low temperatures have been observed in doped semiconductors and many amorphous alloys, however.[10] Recently, Sugihara, Hishiyama, and Kaburagi reported the resistivity and negative transverse magnetoresistance expressed by Eqs. (1) and (2), respectively, for boron-doped natural graphite compacts at rather high temperatures and in a rather strong magnetic field region.[11] Since the crystallinity of the boron-doped specimen is similar to that of pristine natural graphite, they explained the results in terms of the Slonczewski-Weiss-McCure (SWMcC) band model and a weak localization theory obtained by extending Kawabata's theory in a regime of intermediate atomic fraction of boron with an x_B of 1 at. %.[12,13]

The effect of boron doping on rather high doping levels, from 0.5 at. % boron to the limit of its solubility, using well-crystallized graphite materials of large sizes has not been studied systematically. Well crystallized, highly oriented graphite films (HOGF's) prepared from aromatic polyimide films are included in such well-crystallized graphite materials.[14] The aim of the present paper is to study the effect of disorder induced in the graphite layer planes by boron doping on transport properties using boron-doped HOGF's (B-HOGF's) with x_B from 0.4 up to 2.2 at. % B.

II. EXPERIMENT

A. Sample preparation

A 25-μm-thick polyimide film Kapton was used as the starting material for the HOGF of the present study. The HOGF specimens of about 11 μm in thickness were obtained finally by heat treatment at 3000 °C for 1 h. The preparation method for HOGF is given elsewhere.[14]

Boron doping of HOGF's was made as they were sandwiched between polished, commercially available boron-doped artificial graphite plates containing 10 wt. % boron (Toyo Tanso GB110) and then heat-treated in a graphite resistance furnace at 2500 °C for 2 h or 2350 °C for 5 min in a flow of Ar gas. As a result of these treatments, we could dope boron of about 2 at. % into HOGF's. To obtain B-HOGF's with lower boron concentrations, B-HOGF's thus obtained were diluted by a second heat treatment at temperatures of 2450, 2500, 2550 and 2600 °C for 10 sec, while being sandwiched between polished artificial graphite plates without boron. Doping and the second heat-treatment conditions are summarized in Table I.

B. X-ray diffraction and scanning-electron-microscope observation

X-ray diffraction measurements were carried out using a wide-angle diffractometer with a specially designed sample holder for films and Cu $K\alpha$ radiation. Since the graphite layer planes were oriented parallel to the film surface to a high degree for each of the HOGF and B-HOGF's, the 002, 004, and 006 diffraction lines were measured in the reflection mode and the 100 and 110 diffraction lines in the transmission mode. The lattice constant c_0 was determined from the 002, 004, and 006 lines and the constant a_0 from the 100 and 110 lines, referring to the external standard of the thin HOPG specimen with a flat cleaved surface: c_0 of the HOPG specimen was found to be 0.670 70 nm by the powder method with the internal standard of high-purity silicon powder. In order to obtain the effect of boron doping on the preferred orientation of the crystallites, the full width at half maximum of the peak intensity recording of the 002 diffraction plotted as a function of rotation angle φ of the specimen, $\varphi_{1/2}$, was measured for the HOGF and B-HOGF's. $\varphi_{1/2}$ gives information on the degree of orientation of the c axes of constituent crystallites in the film. Cross sections of B-HOGF's were observed by a field-emission gun-type scanning electron microscope (FESEM), which was operated with an acceleration voltage for the primary electron beam of 2 kV.

C. Raman scattering

The Raman-scattering experiments were carried out for the HOGF and B-HOGF's at room temperature in air using the JOBIN YBON RAMANOR T-64000 instrument. For comparison, the measurements of an HOPG and a glasslike carbon heat-treated at 1600 °C (GC-1600) were made. HOPG has high crystallinity with the lattice constants a_0 and c_0 of 0.246 12 nm and 0.670 80 nm, respectively, and $\varphi_{1/2}$ of 0.4°. GC-1600 is a typical disordered carbon having a c_0 of 0.704 nm, an a_0 of 0.242 nm and the same values of crystallite sizes L_a and L_c along the basal plane and c axis, respectively, of 2.0 nm. These values were determined in the

present study by a powder method using Cu $K\alpha$ radiation and an internal standard of high-purity silicon powder. To obtain the values, corrections of the diffraction pattern for Lorentz polarization and atomic scattering and absorption factors were made. Raman scattering signals from cleaved surfaces of the HOPG, HOGF, and B-HOGF and the fractured surface of GC-1600 were recorded with 514.5-nm excitation. The optical power at the sample position was about 10 mW, and 10 h accumulation was employed for each measurement.

D. Transport properties

The transport properties were measured for the HOGF and all B-HOGF's by a dc method. A gold wire of 50 μm diameter was used for electrical leads. Contacts of electrical leads to the specimen were made by gold paint.[14]

The electrical resistivity was measured at 300 K. The dependence of the relative electrical resistivity on temperature was measured in the temperature range of 1.8–300 K. The Hall coefficient R_H and transverse magnetoresistance $\Delta\rho/\rho_0$ were measured at 3.0 K in fields up to 4.2 T using a superconducting magnet. For the measurements, the magnetic field was applied perpendicular to the film surface.

III. RESULTS AND DISCUSSION

A. X-ray diffraction and scanning-electron-microscope observation

The lattice constants a_0 and c_0 for the HOGF and B-HOGF's are listed in Table I. The empirical relations for the lattice constants a_0 and c_0 with respect to the atomic fraction of dissolved boron x_B (in at. %) for Madagascar graphite obtained by Lowell are

$$a_0=(a_0)_{gr}+0.000\,310\,x_B \tag{3}$$

and

$$c_0=(c_0)_{gr}-0.000\,594\,x_B, \tag{4}$$

in nanometers, where $(a_0)_{gr}$ and $(c_0)_{gr}$ are the lattice constants of original Madagascar graphite.[1] The values of $(a_0)_{gr}$ and $(c_0)_{gr}$ obtained by Lowell are 0.246 023 and 0.671163 nm, respectively. Differences in the lattice constants between Madagascar graphite and the HOGF are so small that we may use these equations, replacing $(a_0)_{gr}$ and $(c_0)_{gr}$ with the lattice constants of the HOGF. The x_B values for other B-HOGF's were estimated using relation (4). The values of x_B for B-HOGF's are listed in Table I. The B-HOGF is designated hereafter as B-HOGF followed by a value of x_B. The x_B values obtained for B-HOGF-0.4 and B-HOGF-2.2 using relation (3) are 0.37 and 2.22 at. %, respectively, while those obtained from relation (4) are 0.35 and 2.25 at. %, respectively. Agreement of the x_B values evaluated from two equations is very good.

For the HOGF, only the 002, 004, and 006 diffraction lines have been observed in the reflection mode while the 100 and 110 lines with traces of the 002 and 101 lines in the transmission mode. The 004 and 006 lines are separated into two peaks due to $K\alpha_1$ and $K\alpha_2$ radiations. With increasing x_B, the 002, 004, and 006 lines in the reflection mode for B-HOGF's shift to the higher angles, which is exemplified in Fig. 1 for the 004 diffraction.

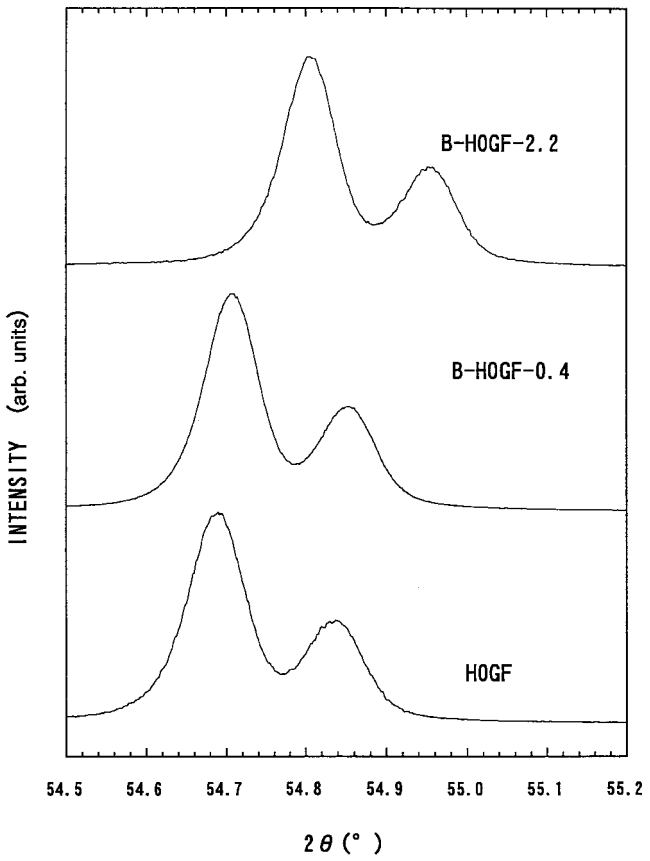

FIG. 1. 004 diffraction patterns of the HOGF, B-HOGF-0.4, and B-HOGF-2.2.

Boron doping slightly disturbs the highly oriented texture in the HOGF. The disturbance in orientation is seen in the 002 peak intensity recordings of the HOGF, B-HOGF-0.4, and B-HOGF-2.2, as shown in Fig. 2. In Fig. 2, the 002 peak intensities for these films are shown, normalizing the maximum intensity to be unified. The values of $\varphi_{1/2}$ for the HOGF, B-HOGF-0.4, and B-HOGF-2.2 are listed in Table I. On the other hand, boron doping causes the 101 and 112 lines to be observable in the transmission mode but not in the reflection mode. The intensities of these lines are quite low, mere traces for the specimen with the lowest value of x_B. They increased with an increase in x_B. The disturbance is so slight, however, with some of the large crystal domains increasing their declining angles of their c axes from the normal to the film surface, that it cannot be detected in the reflection mode but in the transmission mode.

Figure 3 shows the images of the FESEM for cross sections of the HOGF and B-HOGF-2.2. The micrographs of the FESEM images for the cross sections of the B-HOGF's are very similar to those of the HOGF. In the FESEM images of B-HOGF-2.2, extended layer textures are recognized, and small regions of bend layer textures are seen. These regions increase the $\varphi_{1/2}$ value and the appearance of the 101 and 112 lines in the x-ray diffraction patterns in the transmission

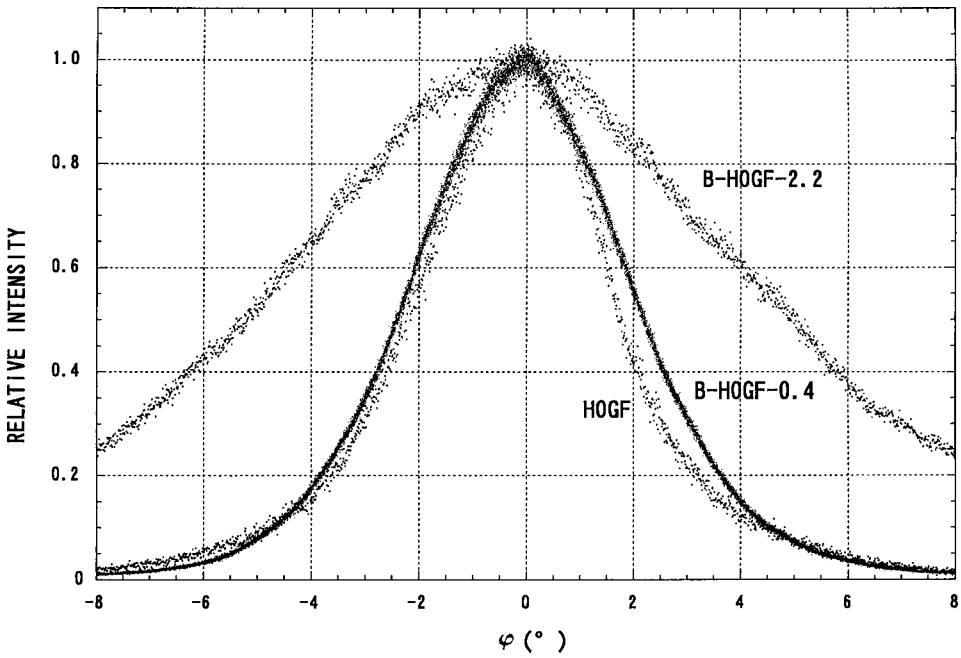

FIG. 2. Peak intensity recordings of 002 diffraction plotted as a function of rotation angle φ for the HOGF, B-HOGF-0.4, and B-HOGF-2.2.

mode. Particles on the specimen surface of B-HOGF-2.2 are residual gold particles of the gold paint used for electrical contacts.

B. Raman scattering

The Raman spectra of HOPG, HOGF, B-HOGF-0.4, B-HOGF-2.2, and GC-1600 in the region between 800 and 3500 cm^{-1} are shown in Fig. 4, taking the peak intensities of the G band to almost the same values.

The Raman spectrum of the present HOPG is the same as that obtained for HOPG by Kawashima and Katagiri.[15] The Raman spectrum of the HOPG shows a G band at 1585 cm^{-1}, an overtone band at 2441 cm^{-1}, G_1' and G_2' bands at 2680 and 2725 cm^{-1}, respectively, and an overtone band at 3249 cm^{-1} ($2D'$ mode). In addition to these bands, the spectrum exhibits weak and distinguishable bands at 1048, 1758, 1846, and 3186 cm^{-1}, though the intensity scale is not enlarged enough to see them. For the HOGF, a spectrum similar to that of HOPG has been obtained but the HOGF exhib-

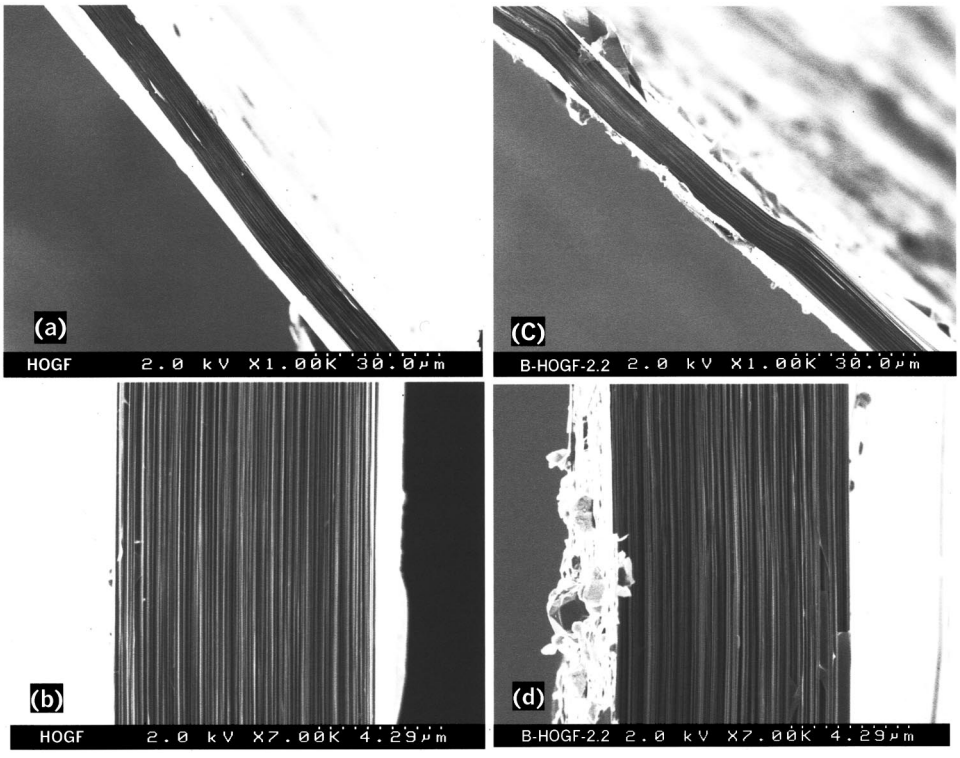

FIG. 3. FESEM images for cross sections of (a, b) HOGF and (c, d) B-HOGF-2.2.

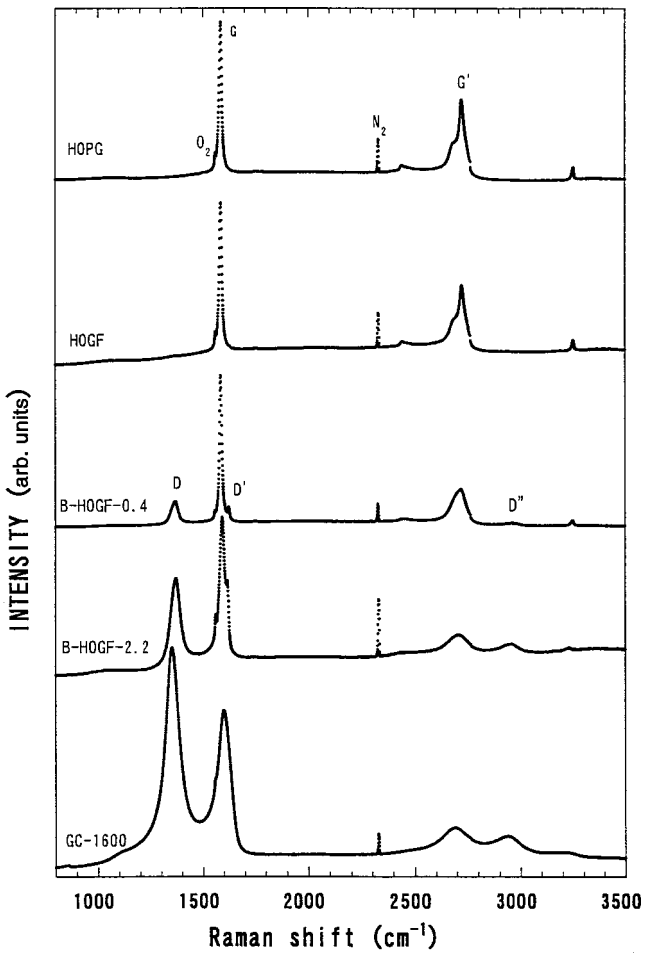

FIG. 4. Raman spectra of the HOPG, HOGF, B-HOGF-0.4, B-HOGF-2.2, and GC-1600 with 514.5-nm excitation.

its a very weak D band at 1372 cm^{-1}. The crystallinity of the HOGF is less perfect than that of HOPG. Assignments of the peaks for the HOPG and HOGF according to Kawashima and Katagiri are listed in Table II.[15]

As shown in Fig. 4, the spectra of B-HOGF-0.4 and B-HOGF-2.2 are similar to those of carbon materials with small crystallites.[5] For B-HOGF-0.4, the spectrum shows the relatively strong D band (1367 cm^{-1}), the D' band (1623 cm^{-1}) at the high-frequency side of the G band (1584 cm^{-1}), the single unsymmetrical G' band (2720 cm^{-1}), which is a merged band of G' and G'' bands (observed in HOPG and the HOGF), the D'' band (2962 cm^{-1}), and the $2D'$ band (3246 cm^{-1}). The D band is assigned to first-order scattering from a Brillouin-zone-boundary phonon activated by the disorder associated with the small crystallite boundary or boundaries of larger crystallites.[3] This assignment is supported by the observation of the G' band ($2725\,cm^{-1} \sim 2\times 1367\,cm^{-1}$) in the second-order Raman spectrum[4] of HOPG and also the present HOPG and HOGF. The D' band is identified with the high density of states for midzone phonons near the maximum phonon frequency and the $2D'$ band is assigned to be a counterpart in the second-order spectrum of this band.[4,6] The D'' band is assigned to a combination of the D and G bands ($2962\,cm^{-1} \sim 1367 + 1584\,cm^{-1}$).[4] The appearance of the D, D', and D'' bands is a characteristic of the disordered graphite structure and related to the substituted boron atoms in graphite layer planes.

The spectrum of B-HOGF-2.2 in Fig. 4 indicates that with increasing x_B the intensities of the D and D' bands relative to the G band increase and that of the G' band decreases. Since the x-ray diffraction profiles in the transmission mode show the quite narrow 101 and 112 diffraction lines, it is worthwhile to note that degrees of the crystallinity of these materials are still high. As shown in Fig. 4, the Raman spectrum of GC-1600 is similar to that of B-HOGF-2.2, showing a higher disorder.

C. Transport properties

Figure 5 illustrates the SWMcC bands,[13] where E_{1+} and E_{2+} are electron bands, while E_{1-} and E_{2-} denote hole bands. We suppose that the SWMcC bands were not affected by boron doping. Since the Fermi energy E_F is located far below the E_3 level for B-HOGF's, there are two hole Fermi surfaces corresponding to the majority E_1 band and minority E_2 band. These Fermi surfaces are schematically shown in Fig. 6.

According to the SWMcC band model,[13] we can relate the majority holes per carbon atom h_{maj}/C and also the minority holes per carbon atom h_{min}/C to the Fermi energy E_F by the following equations:

$$\frac{h_{maj}}{C} = \frac{1}{\sqrt{3}\pi^2\gamma_0^2}\int_0^{\pi/2} d\phi\{E_F^2 - E_F(E_1+E_3)+E_1E_3\}, \quad (5)$$

$$\frac{h_{min}}{C} = \frac{1}{\sqrt{3}\pi^2\gamma_0^2}\int_{\phi_0}^{\pi/2} d\phi\{E_F^2 - E_F(E_2+E_3)+E_2E_3\}. \quad (6)$$

In these equations,

$$E_1 = \Delta + 2\gamma_1\cos\phi + 2\gamma_5\cos^2\phi,$$

$$E_2 = \Delta - 2\gamma_1\cos\phi + 2\gamma_5\cos^2\phi,$$

$$E_3 = 2\gamma_2\cos^2\phi, \quad \phi = c_0k_z/2,$$

c_0 is the lattice constant and ϕ_0 is the value of ϕ at the crossing point of E_F and E_2 and equals 1.01 rad (57°). γ_0, γ_1, γ_2, γ_3, γ_5, and Δ denote the band parameters. To obtain Eqs. (1) and (2), we set $\nu \equiv (2\gamma_4/\gamma_0)\cos\phi \ll 1$. We obtain holes per carbon atom h/C as the sum of Eqs. (5) and (6), using the values of the band parameters as follows:[16]

$$\gamma_0 = 3.16\,eV, \quad \gamma_1 = 0.39\,eV,$$

$$\gamma_2 = -0.020\,eV, \quad \gamma_4 = 0.044\,eV,$$

$$\gamma_5 = 0.038\,eV, \quad \Delta = -0.008\,eV.$$

Since the calculated value of h/C is related to x_B, the values of h_{maj}/C, h_{min}/C and E_F are obtained as listed in Table III.

The room-temperature electrical resistivity $\rho_{300\,K}$, the resistivity ratio $\rho_{300\,K}/\rho_{3\,K}$ where $\rho_{3\,K}$, the resistivity at 3.0 K,

TABLE II. Peak position of Raman spectra in units of cm^{-1} for the HOPG, HOGF, B-HOGF-0.4, B-HOGF-2.2, and GC-1600 with 524.5-nm excitation. Assignments are from Kawashima and Katagiri (Ref. 15).

HOPG	HOGF	B-HOGF-0.4	B-HOGF-2.2	GC-1600	Assignment
		853	853	853	
1048	1046	1050	1054	1100	
	1372	1367	1369	1351	D
1560	1559	1557	1560	1560	Atmospheric O_2
1585	1585	1584	1591	1599	G
		1623	1616		D'
1758	1754	1753	1751		
1846	1864	1860			
2331	2331	2328	2330	2328	Atmospheric N_2
2441	2443	2446	2430		$1053+D$
2725	2725	2720	2708	2691	$2D$ (G')
		2962	2946	2940	$D+G$ (D'')
3186	3186	3180	3162		$2G$
3249	3249	3246	3229	3246	$2D'$

and transverse magnetoresistance at 3.0 K in a magnetic field of 1 T, $(\Delta\rho/\rho_0)_{3\,\mathrm{K},1\,\mathrm{T}}$, for the HOGF and B-HOGF's are listed in Table I. The HOGF is characterized by a large value of $(\Delta\rho/\rho_0)_{3\,\mathrm{K},1\,\mathrm{T}}$, while each of B-HOGF's is differentiated by a small positive or a small negative value of $(\Delta\rho/\rho_0)_{3\,\mathrm{K},1\,\mathrm{T}}$.

Values of $\rho_{300\,\mathrm{K}}$ and $\rho_{3\,\mathrm{K}}$ for the HOGF and B-HOGF's are plotted against x_B in Fig. 7. At any temperature, the resistivity increases with increasing x_B. The dependence of the resistivity ρ_T on temperature for the HOGF is weakened at the lowest x_B value in the present study, while keeping the weak dependence for all of B-HOGF's. This fact indicates that scattering from the substituted boron atoms dominates over the lattice scattering.[7]

Figure 8(a) shows the relative resistivity $\rho_T/\rho_{300\,\mathrm{K}}$ for the HOGF plotted as a function of temperature T. The dependence of ρ_T on temperature for the HOGF is quite similar to that of the graphite whisker of the highest crystallinity,[17] indicating a high degree of the crystallinity of the HOGF. The Hall coefficient R_H and transverse magnetoresistance $\Delta\rho/\rho_0$ for the HOGF as a function of magnetic field B are shown in Figs. 8(b) and 8(c), respectively. R_H of the HOGF is negative and Shubunikov–de Haas oscillations superpose on the field dependence of R_H and also on that of $\Delta\rho/\rho_0$, showing again the high degree of crystallinity of the HOGF.

Values of $\rho_T/\rho_{300\,\mathrm{K}}$ for B-HOGF's are plotted as a function of $\sqrt{T}$ in Fig. 9. In the figure, the number represents the value of x_B. As described above, all B-HOGF's show very weak temperature-dependent resistivity and exhibit systematical changes in the resistivity against $\sqrt{T}$. With increasing $\sqrt{T}$, starting from the lowest temperature, the resistivity decreases linearly with $\sqrt{T}$ but gradually up to about 20 K at

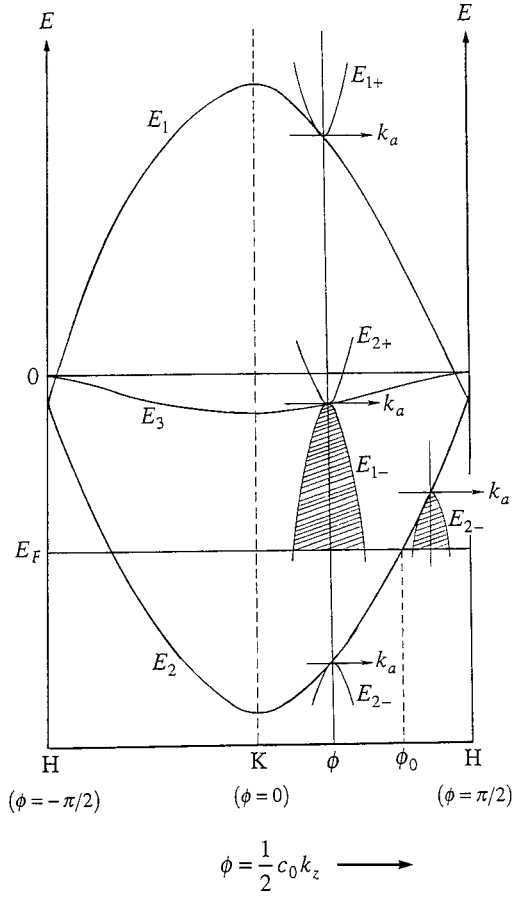

FIG. 5. Illustration of the Slonczewski-Weiss-McClure (SWMcC) band.

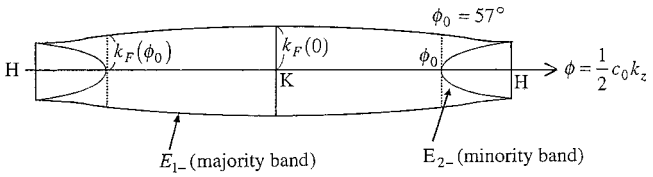

FIG. 6. Schematic drawing of the Fermi surfaces for B-HOGF's.

TABLE III. Values of majority holes per carbon atom h_{maj}/C, minority holes per carbon atom h_{min}/C, and Fermi energy E_F calculated by the SWMcC band model for B-HOGF's.

Sample	$\frac{h_{\mathrm{maj}}}{C}$	$\frac{h_{\mathrm{min}}}{C}$	E_F (eV)
B-HOGF-0.4	0.0037	0.0003	−0.44
B-HOGF-0.5	0.0046	0.0004	−0.50
B-HOGF-0.9	0.0079	0.0011	−0.71
B-HOGF-1.4	0.012	0.002	−0.92
B-HOGF-2.2	0.018	0.004	−1.18

first, continues to decrease a little bit steeply, passes through a shallow minimum, and then increases. The temperature at which the resistivity minimum appears increases with increasing x_{B}, exceeding 300 K for B-HOGF-1.4 and −2.2. The low-temperature resistivity can be written by Eq. (1). Since the temperature dependence of the resistivity for each of the B-HOGF's is very weak, Eq. (1) can be related to the additional resistivity superimposed on the Boltzmann contribution. The additional resistivity is possibly attributed to the quantum correction of the resistivity due to the 3D weak localization $\delta\rho$, which is obtained by Sugihara, Hishiyama, and Kaburagi, extending Kawabata's theory to the SWMcC band.[11] Equation (A1) in the Appendix gives their calculated results, showing $\delta\rho \propto \sqrt{T}$.

The Hall coefficient R_H measured at 3.0 K for B-HOGF's is plotted as a function of magnetic field B in Fig. 10. The values obtained for B-HOGF-1.4 are not shown in the figure, but they are very close to those measured for B-HOGF-2.2. Expected behaviors of the field dependence of R_H from the calculated values of h_{maj}/C and h_{min}/C for B-HOGF's are as follows: R_H is positive and with increasing magnetic field it decreases at first and levels off in the high-field region. The high-field values are related to h/C by the following equation:

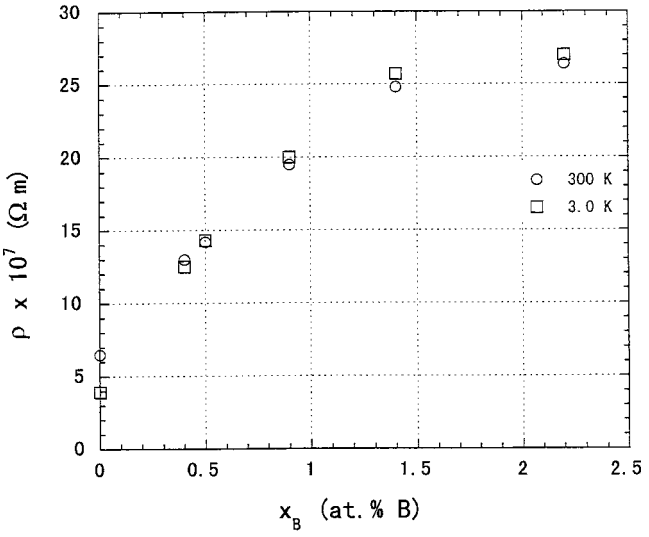

FIG. 7. Resistivities $\rho_{300\,\mathrm{K}}$ and $\rho_{3\,\mathrm{K}}$ for the HOGF and B-HOGF's plotted as a function of the atomic fraction of boron x_{B}.

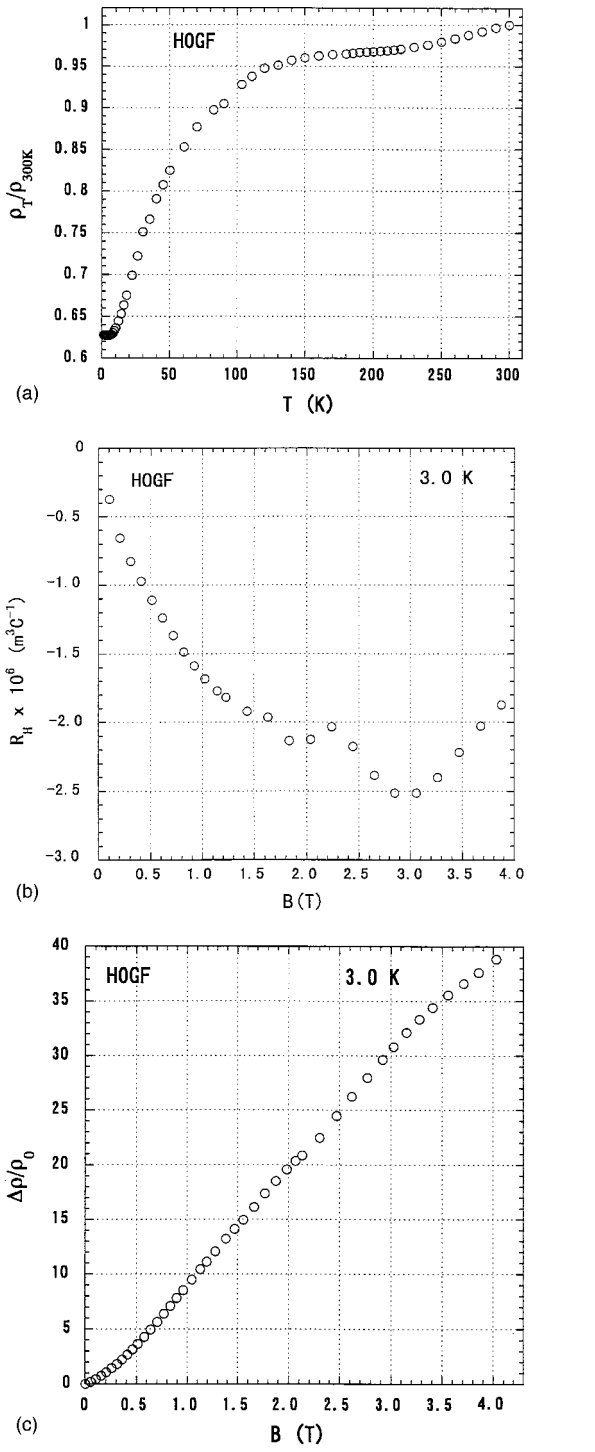

FIG. 8. Relative resistivity $\rho_T/\rho_{300\,\mathrm{K}}$ plotted as a function of (a) temperature T, and (b) Hall coefficient R_H, and (c) transverse magnetoresistance $\Delta\rho/\rho_0$ measured at 3.0 K plotted as a function of magnetic field B for the HOGF.

$$[R_H]_{B\to\infty} = \frac{1}{(n_{\mathrm{min}} + n_{\mathrm{maj}})e}. \tag{7}$$

In Eq. (7), n_{min} and n_{maj} are densities of the minority and majority holes, respectively. The observed behavior for B-HOGF-0.4 is completely different from that expected, and

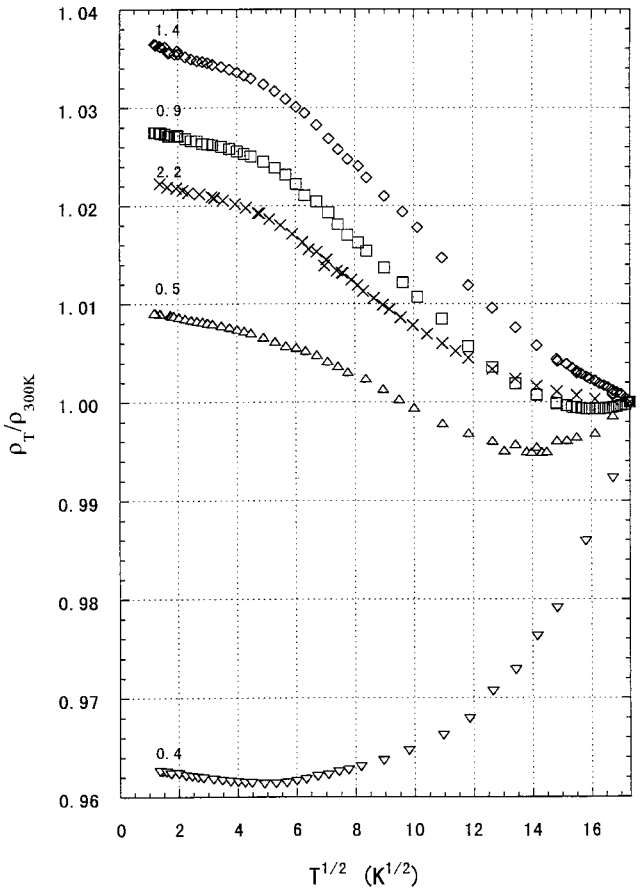

FIG. 9. Relative resistivity $\rho_T/\rho_{300\,\mathrm{K}}$ for B-HOGF's plotted as a function of $\sqrt{T}$.

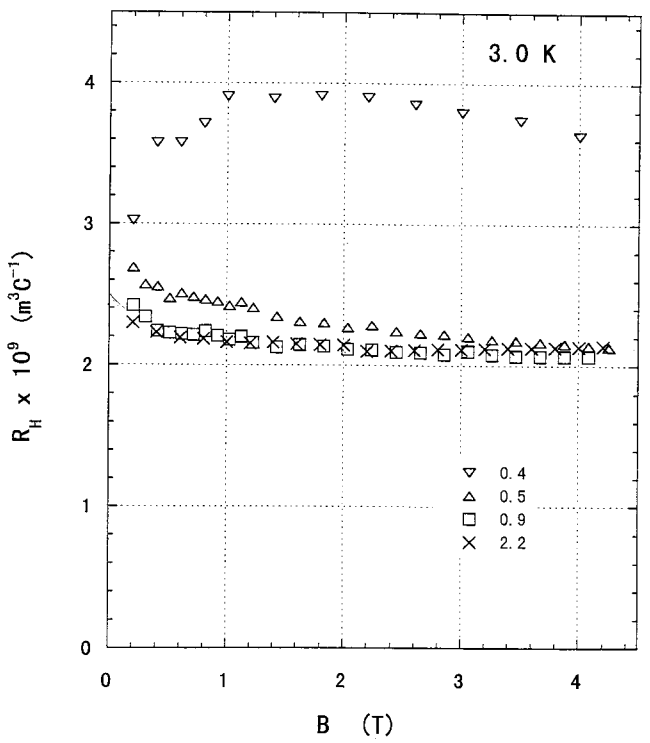

FIG. 10. Hall coefficient R_H measured at 3.0 K for B-HOGF's plotted as a function of magnetic field B.

the expected high-field value of $(R_H)_{\mathrm{exp}}$ by Eq. (7) for each of the B-HOGF's is higher than that observed $(R_H)_{\mathrm{obs}}$ as listed in Table IV. The difference between $(R_H)_{\mathrm{exp}}$ and $(R_H)_{\mathrm{obs}}$ however, becomes smaller with increasing x_{B}. Since the Hall coefficient is proportional to the Hall voltage, the difference may be due to the cancellation of the Hall voltages of the different sign. We note the Hall coefficient of the HOGF at 3.0 K is negative and field dependent, and its absolute values are 2–3 orders of magnitude larger than those for B-HOGF's [Fig. 8(b)]. The cancellation of the Hall voltages is probably due to inhomogeneous boron doping in each of the B-HOGF's. B-HOGF's other than B-HOGF-2.2 were prepared by dilution of boron contained in the materials similar to B-HOGF-2.2, i.e., by a second heat treatment at temperatures between 2450 and 2600 °C for 10 sec, as described in sample preparation. The second heat treatment not only dilutes the atomic fraction of boron of the B-HOGF but also possibly creates a small amount of crystal grains of graphite, which contain few boron atoms. The resultant B-HOGF is probably mixed crystal grains with and without boron atoms. The grains without boron atoms are distributed among the grains with boron atoms. By flowing an electrical current and application of a magnetic field, a negative Hall voltage with a large absolute value is generated in each crystal grain without boron atoms and a small positive Hall voltage in that with boron atoms. The amount of the crystal grains without boron atoms is possibly so small even for B-HOGF-0.4 that the x-ray diffraction lines related to the crystal grains of graphite cannot be detected and the temperature dependence of the resistivity is not affected by existence of such crystal grains. The amount may possibly decrease with increasing x_{B}. In this conjecture, the atomic fraction of boron for each of the B-HOGF's is hard to obtain from the Hall coefficient result. However, since in B-HOGF-2.2 the difference in $(R_H)_{\mathrm{exp}}$ and $(R_H)_{\mathrm{obs}}$ is the smallest, its Hall coefficient result seems to exhibit the field dependence of the Hall coefficient for a B-HOGF with x_{B} close to the solubility limit.

Figure 11 shows the transverse magnetoresistance $\Delta\rho/\rho_0$ measured at 3.0 K for the B-HOGF's plotted as a function of $\sqrt{B}$. For B-HOGF-1.4 and -2.2, $\Delta\rho/\rho_0$ is negative and decreases with increasing $\sqrt{B}$. For B-HOGF-0.4, -0.5, and -0.9, $\Delta\rho/\rho_0$ is negative in low fields, decreases with increasing $\sqrt{B}$ at first, passes through a minimum, and increases with a change in the sign. The magnetic field for the minimum or the field with the change of the sign of $\Delta\rho/\rho_0$ increases with increasing x_{B}. The $\Delta\rho/\rho_0$ values for B-HOGF-0.4 and -0.5 in a field of 4.0 T are not shown in the figure, the values are 3.38% and 1.57%, respectively. These results indicate further increase of the positive transverse magnetoresistance with increasing magnetic field. The positive transverse magnetoresistance is measured for well-crystallized graphite materials such as natural single crystals, HOPG and HOGF, etc., which is due to the mixed electron and hole carrier conduction and proportional to B^n with n close to 1.8.[18] The positive transverse magnetoresistance is measured as the voltage change in the electric resistance by application of magnetic

TABLE IV. Expected values of the high-field Hall coefficient $(R_H)_{\rm exp}$ from $x_{\rm B}$ and $(R_H)_{\rm obs}$ at 3.0 K.

	B-HOGF-0.4	B-HOGF-0.5	B-HOGF-0.9	B-HOGF-1.4	B-HOGF-2.2
$(R_H)_{\rm exp}$ $(10^9\ {\rm m^3\,C^{-1}})$	13.3	10.5	6.18	3.95	2.48
$(R_H)_{\rm obs}$ $(10^9\ {\rm m^3\,C^{-1}})$	3.64	2.14	2.05	2.14	2.14

field, and the voltage change is obtained as the result of the cancellation of the positive and negative changes when the positive changes are larger than the negative changes. The positive changes are attributed to the crystal grains of graphite and the negative changes to the grains in which boron atoms were substituted. The appearance of the positive transverse magnetoresistance in B-HOGF-0.4 and -0.5 gives evidence for the inhomogeneous boron doping mentioned above for the Hall coefficient results, i.e., these B-HOGF's can be regarded as mixed crystals. Though the positive transverse magnetoresistance is not observed for B-HOGF-0.9 in the present magnetic field range, the result indicates the change of sign of the transverse magnetoresistance to occur in the field of about 4.4 T, and this B-HOGF can also be regarded as a mixed crystal.

For B-HOGF-1.4 and -2.2, $\Delta\rho/\rho_0$ decreases linearly with $\sqrt{B}$ in fields above about 0.8 T, i.e.,

$$\Delta\rho/\rho_0 = c - b\sqrt{B}, \tag{8}$$

where c is a positive constant. Equation (8) is not the relation in low fields but in rather high fields. With a further increase of magnetic field, $\Delta\rho/\rho_0$ must saturate in very high fields if it is due to the 3D weak localization. The dependence of the negative transverse magnetoresistance in proportion to $\sqrt{B}$ is observed for B-HOGF-0.9 in fields below 0.41 T, as shown in Fig. 12. If we take note of the field dependence of the transverse magnetoresistance for the crystal grains of graphite, the contribution of these crystal grains to the transverse magnetoresistance of B-HOGF-0.9 can reasonably be negligible in fields below 0.41 T. Accordingly, the negative transverse magnetoresistance observed in low fields for this B-HOGF is substantially characterized by Eq. (2). Since there are, however, similarities among the curves of the field dependence of $\Delta\rho/\rho_0$ for B-HOGF-0.4, -0.5, and -0.9, we assume that Eq. (2) is applicable for these B-HOGF's in low fields. Equation (2) is qualitatively explained by Eq. (A2), which is obtained by Sugihara, Hishiyama, and Kaburagi, extending Kawabata's theory to the SWMcC band.[11]

IV. SUMMARY

Boron-doped graphite films (B-HOGF's) have been prepared from well-crystallized highly oriented graphite films (HOGF's). The following is a summary of the present study.

(1) B-HOGF's are substantially composed of well-crystallized grains. Boron doping disturbs the highly oriented texture in the HOGF, but the disturbance is very slight.

(2) The HOGF shows a Raman spectrum very similar to that of HOPG. Boron doping causes the Raman bands characteristic of graphite materials with lattice disorder. Increasing atomic fraction $x_{\rm B}$ enhances the lattice disorder.

(3) The electrical resistivity increases with increasing $x_{\rm B}$. Boron doping weakens the temperature dependence of the

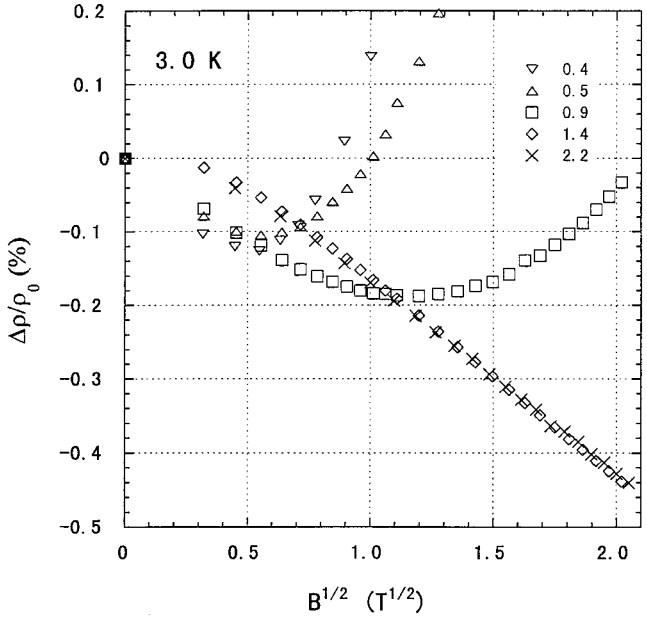

FIG. 11. Transverse magnetoresistance $\Delta\rho/\rho_0$ measured at 3.0 K for B-HOGF's plotted as a function of $\sqrt{B}$.

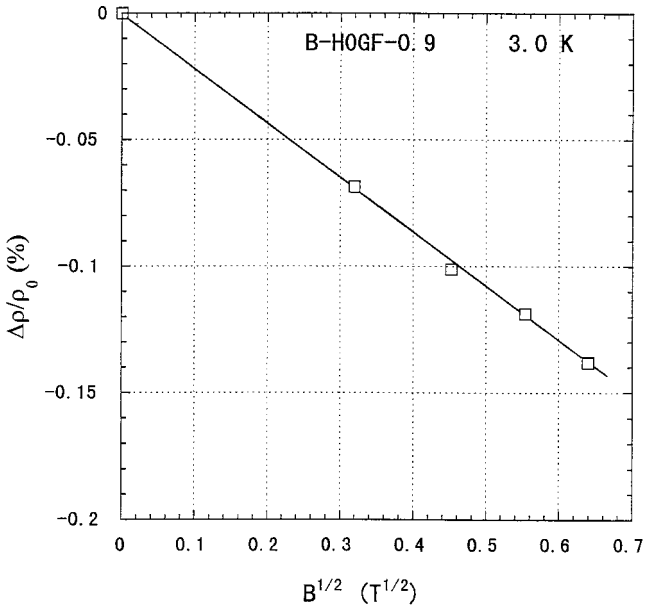

FIG. 12. Square-root B dependence of transverse magnetoresistance measured for B-HOGF-0.9 in fields below 0.41 T at 3.0 K.

resistivity, but the resistivity changes systematically with increasing x_B in a range 1.8–300 K. At low temperatures, the $-\sqrt{T}$-dependent resistivity is observed, which is possibly explained by a characteristic ascribed by the 3D weak localization.

(4) The Hall coefficient R_H measured at 3.0 K for each of the B-HOGF's is positive. The values of R_H for B-HOGF's with x_B of 0.9 at. % boron and below indicate that they are mixed crystals of grains with and without boron atoms.

(5) For B-HOGF's with x_B of 0.9 at. % boron and below, the field dependence of the transverse magnetoresistance also indicates existence of the crystal grains with and without boron atoms. The negative transverse magnetoresistance for these B-HOGF's decreases with $\sqrt{B}$, possibly explained by the 3D weak localization.

ACKNOWLEDGMENTS

The authors thank Professor M. Inagaki of Aichi Institute of Technology, K. Sugihara of Nihon University, and Professor E. Madeen and Dr. Yoshida of the Musashi Institute of Technology for helpful discussions. This research was partially supported by the Ministry of Education, Science, Sports and Culture, Grant-in-Aid for Scientific Research on Priority Areas (Carbon Alloys), 09243101, 1997.

APPENDIX

In disordered electronic systems, constructive quantum interference between elastically backscattered partial carrier waves known as weak localization occurs.[19–21] Weak localization is a low-temperature effect, because inelastic scattering processes due to electron-phonon or electron-electron interactions make the phase incoherence between carrier waves. Experimentally, the weak localization superimposes on the electrical resistivity of the Boltzmann contribution as an additional one, giving rise to a small increase in electrical resistivity with decreasing temperature. The coherence of the backscattered waves tends to be suppressed when the magnetic field is applied, i.e., the weak localization becomes ineffective and a negative magnetoresistance is observed. The quantum correction of the resistivity caused by the 3D weak localization $\delta\rho$ due to extension of Kawabata's theory to the SWMcC band calculated by Sugihara, Hishiyama, and Kaburagi[11] is

$$\frac{\delta\rho}{\rho(0)} = -\frac{2\sqrt{2}}{\pi^4\hbar g(E_F)}\frac{1}{\sqrt{\bar{l}\bar{l}_\varepsilon}}\frac{1}{\sqrt{D_a D_c}}, \tag{A1}$$

$$\overline{D_a} = \frac{1}{2}\overline{v_a^2}\tau, \quad \overline{D_c} = \overline{v_c^2}\tau,$$

$$\mathbf{v} = (\mathbf{v}_a, v_c), \quad \bar{l} = \overline{v_a\tau}, \quad \bar{l}_\varepsilon = \overline{v_a\tau_\varepsilon},$$

where $\rho(0)$ is the in-plane resistivity at 0 K, e is the proton charge, $g(E_F)$ is the density of state at E_F, v_a and v_c are the velocity components of holes in the basal planes and along the c axis, respectively, $\bar{l}$ is the average mean free path for the elastic scattering, and $\bar{l}_\varepsilon$ is the average mean free path for the inelastic scattering. l_ε or τ_ε is associated with the scattering process due to the out-of-plane vibrations and $\bar{l}_\varepsilon \gg \bar{l}$. In Eq. (A1) $\bar{l}_\varepsilon$ is the only T-dependent term, which is proportional to T^{-1} (Ref. 22), and we have $\delta\rho \propto \sqrt{T}$.

The negative transverse magnetoresistance term represented by Eq. (2) can also be calculated as follows:

$$\frac{\Delta\rho}{\rho_0} = -\rho(0)\frac{e^2F}{4\pi^2\hbar l_B A}, \quad F = 0.6, \quad A = \sqrt{2\overline{v_c^2}/\overline{v_a^2}}, \tag{A2}$$

In Eq. (A2), l_B denotes the magnetic length given by $\sqrt{\hbar/eB}$ and $A = 0.24$ obtained by using the SWMcC band model. Therefore, the negative transverse magnetoresistance is proportional to $\sqrt{B}$. Equation (A2) is valid if the following condition is satisfied:

$$\bar{l} \ll L_B \ll L_\varepsilon, \quad L_B = \sqrt{\hbar/4eB}, \quad L_\varepsilon = \sqrt{l\,l_\varepsilon}. \tag{A3}$$

[1] C. E. Lowell, J. Am. Ceram. Soc. **50**, 142 (1967).
[2] T. Hagio, M. Nakamizo, and K. Kobayashi, Carbon **27**, 259 (1989).
[3] F. Tuinstra and J. L. Koenig, J. Chem. Phys. **53**, 1126 (1970).
[4] R. J. Nemanich and S. A. Solin, Phys. Rev. B **20**, 392 (1979).
[5] R. P. Vidano, D. B. Fischbach, L. J. Wills, and T. M. Loehr, Solid State Commun. **39**, 341 (1981).
[6] T. C. Chieu, M. S. Dresselhaus, and M. Endo, Phys. Rev. B **26**, 5867 (1982).
[7] D. E. Soule, in *Proceedings of the Fifth Conference on Carbon* (Pergamon, Elmsford, NY, 1962), Vol. 1, p. 13.
[8] Y. Hishiyama, S. Mrozowski, and A. S. Vagh, Carbon **9**, 367 (1971).
[9] Y. Koike, S. Morita, T. Nakanomyo, and T. Fukase, J. Phys. Soc. Jpn. **54**, 713 (1985).
[10] P. A. Lee and T. V. Ramakrishnan, Rev. Mod. Phys. **57**, 287 (1985).
[11] K. Sugihara, Y. Hishiyama, and Y. Kaburagi, Mol. Cryst. Liq. Cryst. Sci. Technol., Sect. A **340**, 367 (2000).
[12] A. Kawbata, J. Phys. Soc. Jpn. **49**, 628 (1980).
[13] J. C. Slonczewski and P. R. Weiss, Phys. Rev. **109**, 272 (1958); J. W. McClure, *ibid.* **119**, 606 (1960).
[14] Y. Kaburagi and Y. Hishiyama, Carbon **33**, 773 (1995).
[15] Y. Kawashima and G. Katagiri, Phys. Rev. B **52**, 10 053 (1995).
[16] M. S. Dresselhaus, G. Dresselhaus, K. Sugihara, I. L. Spain, and H. A. Goldberg, in *Graphite Fibers and Filaments*, Vol. 5 of the Springer Series in Material Science (Springer, Berlin, 1988).
[17] R. Bacon, J. Appl. Phys. **31**, 283 (1960).
[18] Y. Kaburagi, J. Phys. C **15**, 5425 (1982).

[19] E. Abraham, P. W. Anderson, D. C. Locciardello, and T. V. Ramkrishnan, Phys. Rev. Lett. **42**, 613 (1979).
[20] G. Bergmann, Phys. Rev. B **28**, 2914 (1983).
[21] S. Hikami, A. I. Larkin, and Y. Nagaoka, Prog. Theor. Phys. **63**, 707 (1980).
[22] K. Matsubara, K. Sugihara, and K. Kawamura, J. Phys. Soc. Jpn. **64**, 2558 (1995); S. Ono and K. Sugihara, *ibid.* **21**, 861 (1966).